Water classification using 3D airborne laser scanning point clouds

Michael Vetter, Innsbruck; Bernhard Höfle, Vienna; Martin Rutzinger, Enschede

Dieser Beitrag wurde als „reviewed paper" angenommen.

Abstract

Airborne laser scanning (ALS), also referred to as airborne LiDAR (Light Detection And Ranging), provides highly accurate measurements of the Earth surface. In the last twenty years, ALS has been established as a standard technique for delineating objects (e.g. buildings, trees, roads) and mapping changes. Studies on hydrology or geomorphology such as monitoring of braided river structures, calculation of erosion and accumulation potential in watercourses, or floodplain mapping require all the precise location of the water surface. This paper shows a 3D point cloud based method, which allows an automatic water surface classification by using geometric and radiometric ALS information and the location of modeled lost reflections, which are called laser shot dropouts. The classification result can be used to map the watercourse, to improve DTM filtering routines or to replace water points with river bed heights for hydraulic modeling etc.

The method relies on a threshold based classification using geometry and radiometric information of the 3D point cloud. The method is divided into five major steps. First, we correct the amplitude values by reducing the atmospheric and geometric influences to the laser shots. A radiometric adjustment was applied to the amplitude values of the data sets, which allows multi-temporal analysis of the amplitude values. The second step is the interpolation of the coordinates of the laser shot dropouts, which are the most important input to delineate water surfaces. In step three and four the two attributes (standard deviation of height values and the amplitude density ratio value) are calculated at a fixed distance to each reflection and dropout. These are used in step five to distinguish water and dry land points. The exploration of the attributes for the classification and the evaluation of the classification results are done by comparing the results to a terrestrial orthophoto mosaic an dGPS measurements, which were taken simultaneously to the ALS campaign.

One of the major tasks is the use of modeled laser shot dropouts within a threshold based classification method to distinguish water and non-water echoes. The method is also suited to detect water under riverine vegetation, which is problematic by using data from sensors, that are not able to penetrate vegetation. The classification accuracy is about 95%. The achieved amplitude correction and the radiometric adjustment make the data sets comparable and allow to calculate changes in the channel flow paths within the different flights.

Keywords: LiDAR, airborne laser scanning, laser shot dropout, signal amplitude, multi-temporal analysis, terrestrial orthophoto

Kurzfassung

Airborne Laser Scanning (ALS), auch bekannt als LiDAR (Light Detection And Ranging), liefert Daten der Erdoberfläche in einer hohen Genauigkeit und Punktdichte. Seit den 1990er Jahren entwickelte sich ALS zum Standardverfahren zur Erfassung von Objekten sowie deren Veränderungen, wie beispielsweise Gebäuden, Vegetation oder Straßen. Für Anwendungen in der Hydrologie oder der Geomorphologie wird die Lage der Wasseroberfläche benötigt, die zur Überwachung von Braided-River-Strukturen, der Überflutungskartierung oder für die Berechnung von Erosionsraten von Flüssen herangezogen werden kann. In diesem Artikel wird eine auf der 3D Punktwolke basierende Methode vorgestellt, mit der es möglich ist anhand der geometrischen und radiometrischen Informationen der ALS Daten mit Hilfe von fehlenden Punkten (*dropouts*), Wasserpunkte zu identifizieren und diese zu klassifizieren. Diese Klassifikationsergebnisse können herangezogen werden um Wasserflächen zu kartieren, bestehende Filteralgorithmen zur Geländemodellerstellung zu verbessern oder um Wasserpunkte aus der Punktwolke zu entfernen und diese durch berechnete Flusssohlenpunkte zu ersetzen.

Die Methode besteht aus einer schwellenwertbasierten Klassifikation der Höheninformation und der Radiometriedaten der 3D Punktwolke. Die Methode ist in fünf Hauptschritte aufgeteilt. Als erstes werden die Radiometriedaten (Amplituden) korrigiert, um diese von atmosphärischen und geometrischen Einflüssen zu bereinigen. Anschließend werden diese korrigierten Amplituden verschiedener ALS-Flüge zueinander radiometrisch angepasst, um die Vergleichbarkeit der Datensätze herzustellen. Der zweite Schritt ist die Modellierung von *dropouts*, welche für die Ableitung von Wasserflächen essentiell sind. Als drittes und viertes wird die Standardabweichung der Höhenwerte und

das Amplitudendichteverhältnis für jede Reflexion und jeden *dropout* berechnet. Diese werden bei Schritt fünf zur Unterscheidung von Wasser- und Nicht-Wasserpunkten herangezogen. Zur Ableitung der Schwellenwerte für die Klassifikation wird ein terrestrisches Orthophoto und mit dGPS gemessene Linien verwendet, welche zeitgleich zur ALS Kampagne erhoben wurden.

Ein wichtiger Schritt dieser Methode ist das Einbeziehen der berechneten *dropouts* in die Klassifikation, durch die eine Unterscheidung von Wasser und Nicht-Wasserpunkten ermöglicht wird. Mit der vorgestellten Methode ist auch eine Ableitung von vegetationsüberdeckten Wasserflächen möglich, was bei Sensoren die Vegetation nicht penetrieren können nicht möglich ist. Die Genauigkeit der Klassifikation liegt bei ca. 95% richtig klassifizierten Wasserpunkten. Durch die Korrektur und die Anpassung der Amplitudenwerte wird eine Berechnung der Flusslaufveränderung zwischen den verschiedenen Flügen ermöglicht.

Schlüsselwörter: LiDAR, Flugzeuggestütztes Laserscanning, laser shot dropout, Signalamplitude, multi-temporale Analysen, terrestrisches Orthophoto

1. Introduction

The use of airborne laser scanning (ALS) has developed to the state-of-the-art technique for topographic data acquisition in the last twenty years. Most ALS sensors record the reflected laser beam as X,Y,Z coordinates and the signal amplitude (also referred to as intensity) as a three-dimensional point cloud. Depending on the scanner type, single-, multiple-echoes or even the full-waveform [35] [2] can be recorded. Most ALS driven applications use Digital Surface Models (DSMs) or Digital Terrain Models (DTMs) in raster format computed from the 3D point cloud. To generate those models the point cloud is filtered and classified in e.g. ground, vegetation and building points [31].

Most hydraulic applications use the modeled water surface, derived from a meshed or rasterized DTM, to calculate the volume of the water body, the flow velocity, the floodplain area or to compute flood simulations[24]. The analysis of different ALS data sets makes the monitoring of changes in the watercourse and the flow path of rivers possible. The presented method demonstrates the ability to map water surfaces by using the 3D point cloud information. The calculation of radiometric adjusted amplitude values of multi-temporal ALS data makes the single data sets comparable to each other.

We demonstrate a new approach to distinguish water and non-water echoes from the 3D ALS point cloud by using geometry and signal amplitude values. We use this ALS data instead of optical images or radar data sets because the ALS data provide more information about the surface structure and has the positive effect that ground reflections beyond vegetation are recorded. It is possible to detect reflections (location and amplitude), which are lying on as well as under vegetation. The amplitude values under vegetation are uninterpretable because of the unknown backscattering properties. Furthermore,

the raster interpolation error is not present in point data sets. The advantage of the used data is that land, vegetation and water points can be distinguished. By using radiometric adjusted data sets just one set of classification parameters has to be found because the amplitudes of the different dates are comparable. The results of the presented classification can be used to improve DTM and DSM filtering. Furthermore, the combination of the topographic riverbed information computed from measured river cross sections and the derived water surface is essential to calculate a DTM of the watercourse (DTM-W). Such a DTM-W can be used as basis for hydraulic models [23] [24].

The paper is structured as follows. In section 2, the interaction of laser light in the near infrared wavelength with water and the related work on different water surface delineation methods are discussed. The test sites are presented in section 3 including the reference data production part. In section 4 the amplitude correction and the radiometric adjustment method, the laser shot dropout modeling routine, the data exploration and the classification method are explained. In section 5 the classification results are demonstrated. Finally, in sections 6 and 7 the results are discussed and a conclusion is given.

2. Background
2.1 Interaction of near infrared laser light with water

Electromagnetic waves with 1064~nm wavelength, which are emitted by the Optech's ALTM 3100 [27], have special characteristics when they hit the water surface. Most of the emitted laser pulses are reflected specular on the water surface and a few are absorbed. The reflectance and absorption rate depend on the angle of incidence and the wavelength of the laser light [36] [18]. The incidence angle on water surfaces is almost the same as the scan angle of the laser range vector

because of the low local slope of the water surface. If laser beams have an incidence angle larger than 9°, most of the light reflect specularly, but not in the direction of the ALS receiver, which is the reason for the high number of dropouts [5] [15]. In general, the water surface roughness is not homogeneous because of waves. So the specular reflected laser beam is fragmented into small single reflections. All of them are reflected in different directions because of different angles of incidence, which are a result of the locale slope and the roughness of the water surface within the laser footprint. The Bidirectional Reflectance Distribution Function (BRDF) of water is not Lambertian. Some of those reflections can reach the receiver. If there is not enough energy to detect an echo at the receiver, it won't be recorded (dropout). If there is enough energy at the receiver the echo will be detected at a very low amplitude. Incidence angles near 0° (nadir) most likely lead to specular reflections (i.e. if the water surface is smooth), which causes extremely high amplitude values (section 4.3.1) [15].

2.2 Related work

Various remote sensing techniques are used to delineate water surfaces for floodplain mapping, natural hazard forecasting, water depth measurements, etc. The air- and space borne optical sensors provide the most common and popular data for classifying different land cover classes including water areas [32] [18] [25]. Many features can be derived for water by using the information of multi-spectral optical sensors (e.g. suspended load, proportion of organic material, water depth, etc.) [18]. Optical data are used for land cover classification and monitoring of large areas. The combination of optical data with near-infrared information is a standard method for water surface delineation.

Radar sensors are used for soil moisture mapping, floodplain mapping, water stage modeling etc. (e.g. [10] [32] and [7]). The advantage of using space born radar is the fast revisiting time of the sensor, the global coverage, the high accuracy and spatial resolution of the data especially of TerraSAR-X (SpotLight, 1 m) and the independence of weather situations (especially for tracking the water stage during and after flood events) [30].

In the last few years, measurements with ALS have been established as an additional group of sensors for the data acquisition of the Earth surface. A large number of methods are available for measuring, monitoring and delineating features. ALS data are mostly used to generate Digital Surface Models (DSMs), Digital Terrain Models (DTMs) for the detection of buildings, trees, roads, etc. [22] [34] [28] or to distinguish different surface classes (e.g. snow types) [12]. In bathymetry, ALS systems with two wavelengths are used to measure through the water body to derive the elevation model of underwater objects and the bottom of rivers, lakes, or the ocean [16] [9].

In hydraulics, ALS data are used as raster or triangulated mesh models. Those are the basis for hydraulic models [24]. By generating river bed models out of measured river cross sections [23] [33] the ALS DTM can be modified and updated for hydraulic applications. [3] and [26] show different applications of ALS data for monitoring river environments using rasterized data.

[1] present an object-based classification method for delineating the water surface by using an elevation and an intensity model. They classify water by combining both rasters with near-infrared SPOT images, which have low intensities in the water areas. The delineation accuracy of raster based methods are always in the resolution of the used input models. To compute the location of the water surface only a few methods are established by using the 3D point cloud information [4] [15]. [23] integrate the ALS points and an interpolated river bed model, which is generated from measured river cross sections, to derive the water-land boundary as well as the height of the water surface. Another approach is demonstrated by [4], who use a strip wise classification method by calculating a membership function for each point. As parameters they use the height information, slope, amplitude, missing points (not modeled, only the gap between two reflections) and the point density to classify water and land points in the Wadden Sea. [11] and [14] figured out that the use of corrected signal amplitudes, the standard deviation of height values and modeled dropouts can be used to run a seeded region growing segmentation to derive water surface information. Those methods operate on the 3D point cloud. The results are of high position accuracy and can be used as input for accurate hydraulic models.

3. Test sites and reference data

Three different river sections, which are located in Austria, covered by seven ALS data sets are used in the following study. We use different types of

rivers and various ALS data sets (Tab. 1), with different water conditions, river geometries, morphological parameters, point densities, sensor parameters, vegetation covering, etc. in order to test the parameter settings and to demonstrate the robustness of the method.

3.1 Test sites

The test site at the Hintereisfernerbach is located in the upper Ötztal (Tyrol) at the glacier forefield of the glacier Hintereisferner (46°49'13.77'' N; 10°48'23.58'' E). Five ALS flights are available at this test site, which were taken in the years 2003 to 2007 between August and November [8]. One orthophoto is available from the flight of August 12, 2003 (H03).

This test site was chosen because of the available time series and the special river structure. The Hintereisfernerbach near the glacier is a braided river with a lot of sand and gravel bars in the channel, high suspended load and a turbulent, rough water surface, which makes the classification of water complex.

Data	Date	points/m^2	Altitude [m]
H03	12.08.2003	2.0	1000
H04	05.10.2004	2.0	1000
H05	12.10.2005	2.0	1000
H06	08.10.2006	2.0	800
H07	11.10.2007	2.0	1000
Z07	11.10.2007	1.5	1000
D03	11.09.2003	1.6	728

Data	Scanner	Scan f. [Hz.]	Speed [m/s]
H03	ALTM 2050	30	75
H04	ALTM 2050	30	75
H05	ALTM 3100	40	75
H06	ALTM 3100	41	75
H07	ALTM 3100	41	70
Z07	ALTM 3100	41	70
D03	ALTM 2050	30	70

Data	Angle	PRF [kHz]	Scan w. [m]
H03	20°	50	155
H04	20°	50	155
H05	20°	70	400-600
H06	20°	70	300-600
H07	20°	70	300-600
Z07	20°	70	300-600
D03	30°	20	328-428

Tab. 1: Flight data: H = Hintereisferner (Hintereisfernerbach), Z = Zwieselstein (Venter Ache), D = Doren (Bregenzer Ache); 03 – 07 = year of flight (2003-2007); points/m^2 = mean point density; Altitude = flying altitude above ground; Scan f. = scan frequency; Speed = speed of the aircraft; Angle = maximum scan angle; PRF = pulse repetition frequency; Scan w. = width of the swath

The test site at the Venter Ache is located in Zwieselstein (Ötztal, Tyrol; 46°56'09.17'' N; 11°01'21.53'' E). It is the reference area of the ALS campaign at the Hintereisferner of October 11, 2007 (H07). For this test site a terrestrial orthophoto mosaic was computed (sec. 3.2) which was used to check the relevant attributes for the classification method.

The Venter Ache near Zwieselstein is a torrent with many rocks in the channel. The water surface is characterized by a rough surface and fast flowing channel sections. At the edges of the channel many pools are located, surrounded by gravel and sand, with slow flowing and a smooth water surface.

The Bregenzer Ache is the largest river in the Bregenzerwald (Vorarlberg; 47°28'26.93'' N; 9°51'11.22'' E). The site near Doren was chosen because of the confluence with the Weißache and the lake in the center of the test site.

The Bregenzer Ache is a strongly regulated river and therefore characterized by a smooth water surface. Huge sand and gravel bars inside the Weißache and the Bregenzer Ache are evident, which make the classification process more complex.

3.2 Reference data production

However, orthophotos from aerial images taken parallel to the ALS campaign are rarely available or the resolution of the images is too low.

To analyze the ALS point attributes, it is necessary to know which material (including

water) is hit by the laser beam. The use of orthophotos with higher resolution than the average point distance are a proper method to evaluate and analyze the ALS data. However, orthophotos from aerial images (taken parallel to the ALS campaign) are rarely available or the resolution of the images is too low. Thus, we use a terrestrial orthophoto mosaic with a cell size of 5 cm and a vertical position accuracy of 15 cm.

The workflow of the terrestrial orthophoto generation process is shown in figure 1.
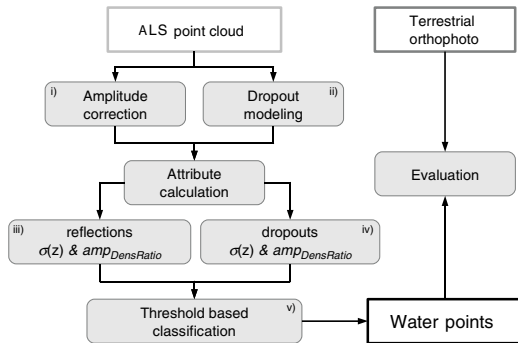
Fig. 1: *Work flow of the classification method;* $\sigma(z) =$ *standard deviation of height values;* $amp_{Dens\,Ratio} =$ *amplitude density ratio*

We took about 50 images of an approximate 70 m long section of the Venter Ache to generate the terrestrial orthophoto. The initial orientation, the bundle block adjustment, the semiautomatic terrain point extraction and the final orthophoto computation are done in *ORPHEUS* [20].

4. Water surface classification

The presented method uses the geometry and amplitude values of the 3D point cloud. The local roughness on water surfaces and bare Earth is very low. The smoothness depends on the water level and on the roughness of the riverbed. The amplitude values are mostly low on water because of the special reflectance and absorption properties (sec. 2.1). By analyzing smooth areas with very low amplitude values, water echoes can be classified (sec. 4.3).

The water surface classification method comprises five major steps (fig. 1). Firstly, a correction and radiometric adjustment for amplitude values (i) and secondly, the locations of laser shot dropouts have to be computed (ii) (sec. 4.1 and 4.2). Next, the roughness parameter (standard deviation of height values) and the amplitude density ratio of each reflection (iii) and each

dropout (iv) are computed at a fixed distance of 2 m (sec. 4.3). By analyzing a part of the laser shot attributes of the Venter Ache by using the terrestrial orthophoto mosaic it is possible to extract the proper information for the classification step (v), which has to be applied to distinguish water and non-water echoes (sec. 4.4). After the classification, the results are evaluated by using all laser shots, which are corresponding to the measured GPS line.

4.1 Amplitude correction and radiometric adjustment

The amplitude correction of each laser shot is necessary to calculate amplitudes, which are almost free of atmospheric and geometric influences. The correction was applied by using the model-driven correction approach of [13]. The used method is derived from the radar equation [17]. The main goal of the amplitude correction is to calculate comparable amplitude values by (a) correcting the different ranges of all laser shots within the different flight strips, (b) accounting for atmospheric attenuation and (c) to normalize the reflection properties [13].

In this study, the amplitudes were corrected to a standard range of 1000 m. The influence of the atmosphere was not corrected because of missing meteorological data. The directional scattering properties of the targets are considered by globally assuming Lambertian scatterers. Although water surfaces exhibit a strong contribution of specular reflection assuming this simple reflectance model was chosen as pragmatic solution for the apriori unclassified laser points. A data-driven solution, for example, is presented in [5] where an empirical model is estimated for the reflectance behavior of water. All data sets were corrected the same way [13].

The radiometric adjustment of amplitudes is necessary to make the amplitude values of each flight campain comparable to each other, when using ALS data sets from different flight campaigns of one test site. For this study we did a radiometric adjustment for the flights at the Hintereisferner (H03-H07). For the two flights at the other test sites (Z07, D03) a radiometric adjustment of the amplitudes can not be realized because at least two different data sets must be available of one site.

The amplitude differences between figure 2a and 2b are the result of different sensors and the relation between flight speed and the pulse repetition frequency (PRF).
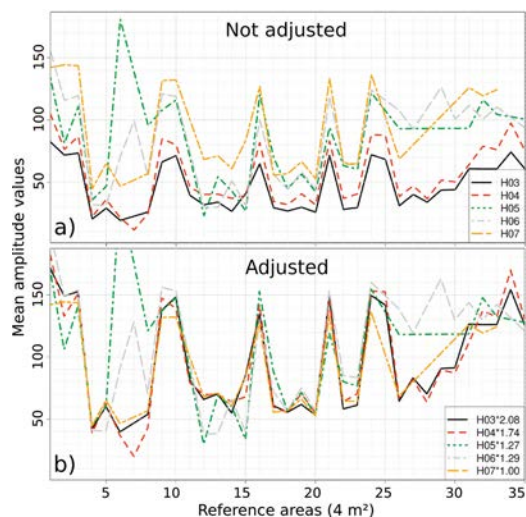
Fig. 2: Radiometric adjustment: a) corrected amplitude values of all data sets (H03 to H07) at the Hintereisferner (mean values of all 35 reference areas, 4 m²); b) radiometric adjusted amplitude values (adjusted to H07, red dashed line), the radiometric adjustment factors are shown in the legend

The radiometric adjustment at the Hintereisfernerbach (H03-H07) was realized by analyzing the amplitude values of the different data sets. Thirty-five reference areas (4 m²) with homogeneous amplitude values are chosen to calculate the radiometric adjustment factor between the data sets (fig. 2). The amplitudes of the points with a scan angle $< 10°$ within each reference area are selected to calculate the mean amplitude value for each reference area. The angle criterion is used to guarantee that all reflections have almost the same scattering properties. By multiplying the corrected amplitude values with the radiometric adjustment factor, the data sets from all flight campaigns at the Hintereisferner (H03 – H06) become comparable and correspond to the amplitude values of the reference data set (H07).

The remaining strong deviations between the strips in figure 2 (reference areas 6 to 8 and 26 to 29 of H05 and H06) can be explained by changing surface conditions compared to the other ALS data (e.g. dry rock instead of wet rock). In figure 3, the reference data set of October 11, 2007 (H07) (fig. 3a) and the data set of October 5, 2004 (H04), (fig. 3b) with corrected amplitudes are shown. The results of the corrected and radiometric adjusted amplitudes of October 5, 2004 (H04) are displayed in figure 3c. The amplitude differences between figure 3a and 3b are the result of different

sensors and campaign settings, which are not corrected by the amplitude correction approach [13]. For the amplitude values of October 5, 2004 (H04), the radiometric adjustment factor is 1.74 (fig. 3c).

Fig. 3: Corrected vs. radiometric adjusted amplitude values: a) corrected amplitudes (October 11, 2007, H07); b) corrected amplitudes (October 5, 2004, H04); c) corrected and radiometric adjusted (the radiometric adjustment factor is 1.74; October 5, 2004, H04); the graphic shows amplitude images (range from 0, black to 160, white)

4.2 Laser shot dropout modeling

A laser shot dropout is a laser shot with no recorded echo. It can occur due to, (i) a specular reflection which is not in the direction of the ALS receiver, (ii) a strong absorption at the reflector or (iii) a lot of reflections on very small areas (foliage in the canopy) in a volume scatterer like a tree with a lot of inside scattering [21]. By using information of the recorded timestamps of the laser shots, the PRF, the IMU and GPS data, the location of each dropout can be calculated (fig. 4).
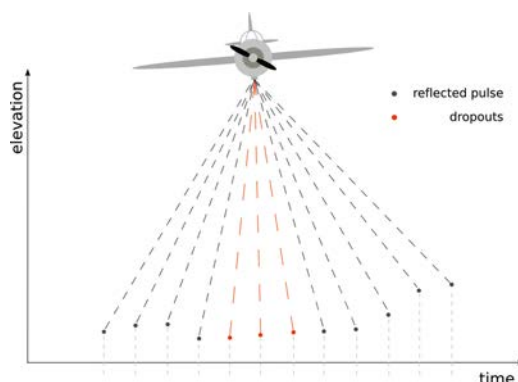
Fig. 4: Dropout modeling schema [14]

To model laser shot dropouts, the time gaps between neighboring points (P_1 to P_2), which are larger than Δt (equation 1) have to be found in the

recorded timestamps (t_{P_1} to t_{P_2}). After finding the time gaps, the number of missing reflections n are calculated (equation 2). At each location where a reflection is missing the X,Y,Z coordinates are calculated (M_i) by using a linear interpolation (equation 3). The amplitude value is set to zero. Uncertainty in elevation leads to rather low vertical accuracy of the interpolated point. Therefore, the height value is not used for calculations but only for visualization.

$$\Delta t[s] = \frac{1}{PRF[Hz]} \qquad (1)$$

$$n = \frac{t_{P_2} - t_{P_1}}{\Delta t} - 1 \quad \text{where}$$
$$n \in N, t_{P_2} > t_{P_1} \qquad (2)$$

$$\overrightarrow{M_i} = \overrightarrow{P_1} + \overrightarrow{P_1 P_2} \cdot \frac{i}{n+1}, \ i = 1, \ldots, n \qquad (3)$$

4.3 Data exploration

To interpret the ALS data and its covered surface, the ALS point cloud is compared to the terrestrial orthophoto mosaic. Differential GPS (dGPS) measurements were acquired at the same time as the ALS campaign. These dGPS measurements are used for the terrestrial orthophoto production and for checking the position of the water-land boundary. The dGPS measured lines are also used for evaluation. The terrestrial orthophoto (fig. 5) is only used for visual inspection.

For checking the amplitude values and the point density on water surfaces (sec. 4.3.1) an independent test site in Innsbruck, which is not listed in table 1, was used. This test site has the advantage that the whole range of scan angles is present within one connected water area (river Inn). The test site at the Venter Ache (Z07) was used to analyze the geometric properties and the local roughness of the point cloud (sec. 4.3.2).

4.3.1 Amplitude values and dropouts

Figure 6 demonstrates the relation between the incidence angle and the signal amplitude on water. The selected points are from two ALS campaigns at the Inn in Innsbruck [15]. The red points are from a summer flight with a lot of suspended load and the blue ones are from fall with clear water conditions. This can also be seen in the different number and strength of the amplitudes in the plot [29]. The summer flight with higher suspended load has a higher backscattering potential than the other, but not a Lambertian [15]. Those data were selected because the Inn is wide enough to guarantee that only water

reflections are within the selection. The visual inspection of the amplitudes at the Venter Ache (Z07, fig. 5) shows the same results as figure 6. Most of the water reflections have very low amplitudes.
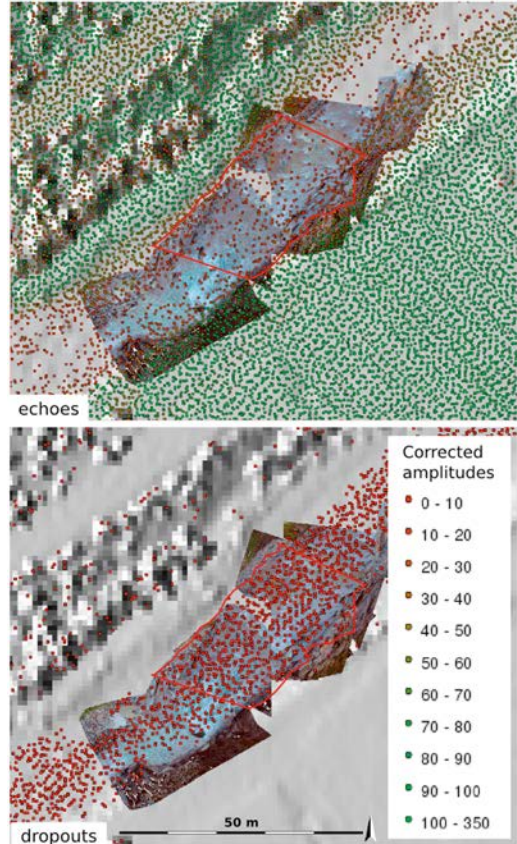
Fig. 5: Terrestrial orthophoto superimposed by the dGPS measured water-land boundary (red line); upper image: corrected amplitudes of the last echoes (October 2007, Z07; color according to corrected amplitudes); lower image: modeled dropouts (colored by the amplitude value of zero)

A decrease of amplitude values is evident from nadir to the end of the scan line (incidence angle with 20°). The point density decreases and therefore the dropouts increase in the direction to the scan edges in a non linear regression [5] [15]. Almost 85 % of the points in figure 6 are lower than an amplitude of 50 and 95 % of all reflections on water are within an incidence angle range between 0° to 10°. Therefore water is characterized by low amplitude values, approximate 10 – 20 % of the whole range of the signal amplitudes (excluding outliers) and a high number of

dropouts [15]. That can also be seen in figure 5. If no reference data set is available, 10 to 20 % of the amplitude range of the whole data set can be used as estimate for the upper threshold in equation 5.
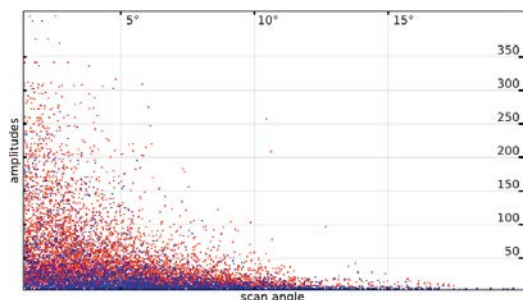
Fig. 6: Relation between angle of incidence (=scan angle) and corrected amplitude values on water (water body at the Inn in Innsbruck in summer 2005, red; in fall 2005, blue) according to [15]

The amplitude density ratio (equation 5) is calculated by modifying the intensity density of [6] (equation 4) by adding the dropout information. The amplitude density ratio $amp_{DensRatio}$ is the relation between the number of echoes with an amplitude value within a defined interval (0 to 50, derived from fig. 6 and fig. 5) $echoes_{AmpValue} < value_{max}\ AND\ echoes_{AmpValue} > value_{min}$ plus the number of $dropouts$ (with an amplitude of zero) divided by the number of $echoes + dropouts$ at a fixed distance of a point (2 m). If there are no dropouts within the search radius, the results of equation 4 and equation 5 are the same. The attribute $amp_{DensRatio}$ can be calculated for both, reflections and dropouts. The $amp_{DensRatio}$ is high if the points, which are surrounding the search point, have low amplitude values and/or most of them are dropouts. If only a few amplitude values are high and most of the points in the search radius are dropouts the $amp_{DensRatio}$ is also high. Both cases are evident on vegetation and on water (fig.7). If no reflection is found within the search radius, the $amp_{DensRatio}$ is 100 %. When all amplitude values are higher than $value_{max}$ and no dropout is found within the search radius, the value is 0 %.

$$amp_{dens} = \frac{echoes_{AmpValue}}{echoes} \cdot 100 \qquad (4)$$

$$amp_{DensRatio} == \frac{dropouts + echoes_{AmpValue}}{dropouts + echoes} \cdot 100 \qquad (5)$$

The information of the $amp_{DensRatio}$ is used for calculating the point density and the relation of low amplitudes plus dropouts to all potential reflections at the same time. The $amp_{DensRatio}$ attribute can be used to distinguish water and vegetation

(with a lot of dropouts) from bare Earth characterized by a very few dropouts (fig. 7).
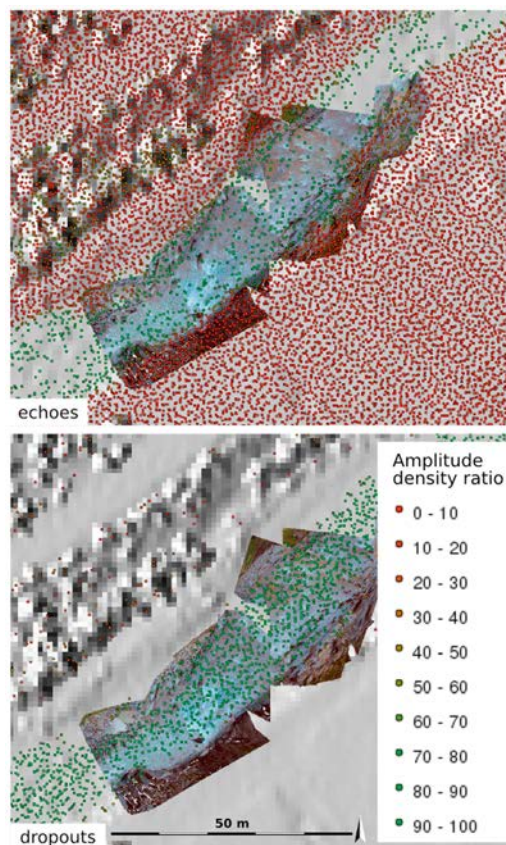
Fig. 7: Calculated amplitude density ratio at the Venter Ache: upper image: echoes; lower image: dropouts; colored by $amp_{DensRatio}$ in %

4.3.2 Geometry values

To remove the vegetation points, which have a high $amp_{DensRatio}$ because of the low reflection properties and a lot of dropouts, the standard deviation of height values $\sigma(z)$ is used.

The profile (fig. 8) shows the elevation variation and the roughness of a river with a sand or gravel bar, river banks and vegetation. By visual inspection, the low roughness of the water surface can be seen.

By using a fixed distance search radius for each point (2 m) the standard deviation of height values $\sigma(z)$ is calculated for each reflection and each dropout.
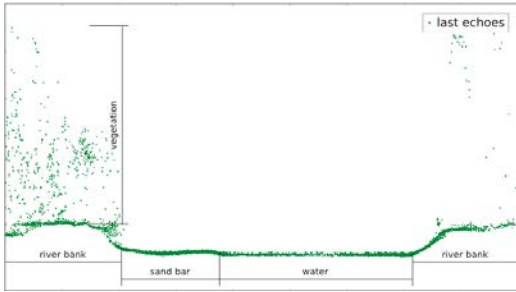
Fig. 8: Profile through a watercourse, showing the elevation values of the ALS point cloud
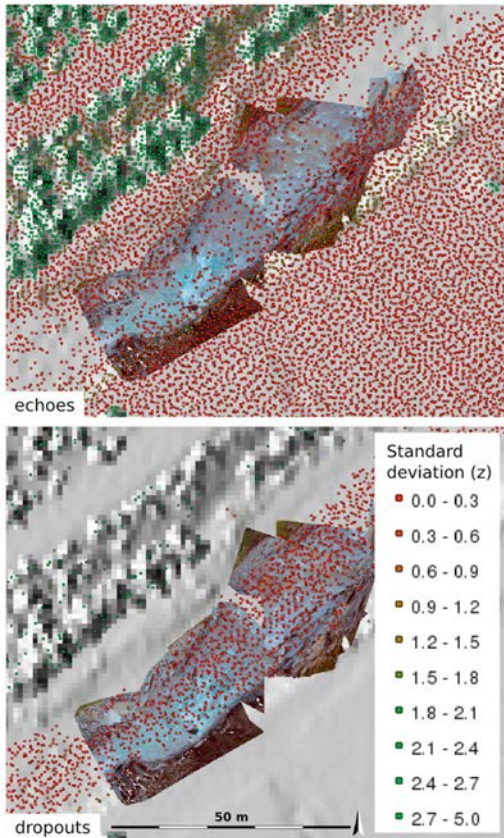
Fig. 9: Standard deviation of height values $\sigma(z)$ at the Venter Ache: upper image: echoes; lower image: dropouts; colored by $\sigma(z)$ in m

The roughness parameters of water surfaces are very different from the surrounding areas of rivers, especially if riverine vegetation is present. In areas with vegetation the local roughness is higher than on bare Earth (e.g. fields) and much higher than on water (fig. 9). The information of the

local roughness can be used for deleting all vegetation points in the classification process. Therefore, the threshold can be figured out with < 0.3 m on rivers with smooth surface and < 0.5 m on rivers, which are rough and steep. The calculation of $\sigma(z)$ is done for both, reflections and dropouts. Sometimes there are no reflections within the search radius around a dropout (especially on water). In this case the $\sigma(z)$ is zero. Only the values of the reflections are used for calculating $\sigma(z)$. The very uncertain height values of dropouts are not used for any calculations only for visualization.

4.4 Threshold based classification

The classification routine uses two different attributes to classify the points into water or non-water. The input attributes are the local roughness $\sigma(z)$ and the amplitude density ratio ($amp_{DensRatio}$, equation 5), which are described in section 4.3. The attribute $\sigma(z)$ is used for classifying horizontal areas (e.g. fields, roads, water) and the $amp_{DensRatio}$ is used to filter out the points with a high dropout rate (water and vegetation). By combining both, water can be localized.
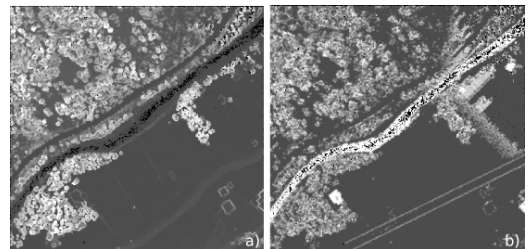
Fig. 10: Pre-classification at the Venter Ache: a) $\sigma(z)$; b) $amp_{DensRatio}$; bright: high value; dark: low value

The thresholds of the attributes are extracted by using a part of the echoes, which represent water in the terrestrial orthophoto mosaic at the Venter Ache. The thresholds of the classification are $\sigma(z) < 0.3$ m and $amp_{DensRatio} > 50\%$ for the class water. The value $\sigma(z)$ depends on the roughness of the water surface. If the surface is smooth the threshold can be set very low, in contrast to a torrent with a rough water surface. The $amp_{DensRatio}$ is set to 50 %. If half of the reflections are on land (higher than the upper threshold) and half are on water (lower or dropouts) the 50 % are fulfilled and the point can be a water point. First, the $\sigma(z)$ attributes (fig. 10a) and then the $amp_{DensRatio}$ values are classified (fig. 10b). If $\sigma(z)$ is lower and the attribute of $amp_{DensRatio}$ is higher than the specific

threshold, the point belongs to water, otherwise to land.

5. Results

The advantage of a 3D point cloud based classification is that the points are not manipulated in their 3D position. By using corrected and radiometrically adjusted amplitude values, the classification parameters have to be calculated only once and can be used for all data sets. The use of the modeled dropouts provides information on objects with no reflections, which is necessary for classifying water surfaces. The result of the Bregenzer Ache (fig. 11a) shows the advantage of using the modeled dropouts to classify water. The center of the test site contains a lake with no ALS returns. The lake can not be classified without the location information of dropouts. In this case, only the modeled dropouts are used to compute the water surface. Each reflection on the lake, which are only a few, are classified as water because of a $\sigma(z)$ of zero and a $amp_{DensRatio}$ of 100 %. The results of the classification at the Venter Ache are shown in figure 11b.

The results at the Hintereisfernerbach show the possibility to apply the method for multi-temporal analysis of the watercourse of a braided river (fig. 12). In multi-temporal analysis the spatial change of the flow paths during the years (fig. 12f) can be computed.

The reference area Venter Ache is used to assess the accuracy of the method by comparing the result with the measured GPS lines. The classification accuracy of the presented method was evaluated by a manual selection of all water reflections at the reference area. All echoes, which are corresponding to the water surface of the measured water-land boundary are selected and compared with the number of classified water points. A comparison of the selected reflections with the calculated water points shows 95 % of correct classified water points. Zero percent of the classified water points are outside the water land boundary (GPS line), which shows that the classification underestimates the water surface area at the present thresholds. Visually the horizontal distance (i.e. underestimation) between GPS line and the outer classified water points lies between 0.5 m and 1 m, indicating that the horizontal accuracy is in the range of the given average point distance.
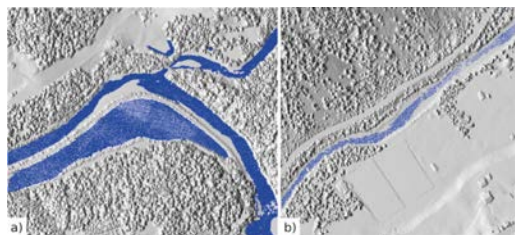
Fig. 11: Classification results: a) Bregenzer Ache, D03; b) Venter Ache, Z07
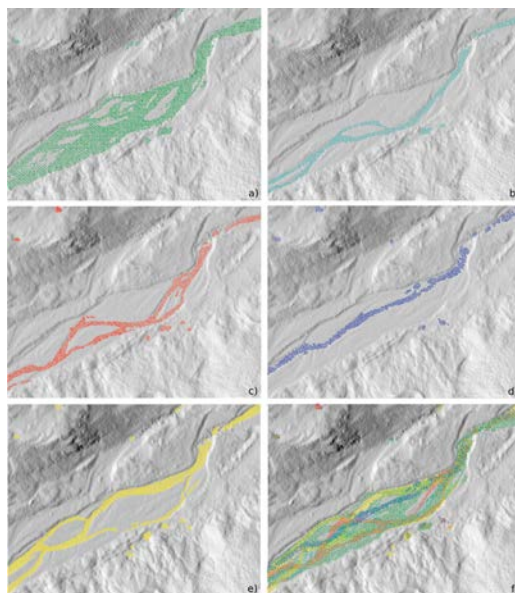
Fig. 12: Classification results at the Hintereisfernerbach: a) August 12, 2003, H03; b) October 5, 2004, H04; c) October 12, 2005, H05; d) October 8, 2006, H06; e) October 11, 2007, H07; f) combination of all classification results

6. Discussion

With the presented dropout modeling method, only dropouts which have two neighbors along the scan line can be modeled. That means that dropouts which are located at the end of a scan line are not detected. In special cases, the end of the scan line is located in a water area and then the used modeling method will be stopped at the last reflection in the scan line.

In the future, the modeling of dropouts has to be improved by a pre-calculation of the scan line locations and an extrapolation method for dropouts to the swath edge. Another method for detecting dropouts is to use the information of the

raw data from the providers. This is possible when providers can record and deliver the whole raw information of the scans, including the timestamps of the non-recorded reflections.

The availability of corrected and radiometric adjusted amplitude values is very important for deriving the water points of multi-temporal data sets because of the comparability of the different data sets.

To improve the comparability of multi-temporal data sets, exactly one flight pattern and one scanner type should be used for all flights in the same area. The radiometric adjustment method can be improved by using radiometric calibration targets (e.g. natural targets measured with a reflectometer). The same targets can be used at each campaign. The known reflectivity of that area can be used for radiometric calibration and adjustment after amplitude correction [2] [19].

The computation time (including point selection, dropout modeling and classification) depends on the selected area and the point density. The use of a raster based flow accumulation for calculating the potential location of rivers and water areas can be implemented as a pre-selection routine to reduce the computation time.

7. Conclusion

The paper presents a method to classify ALS reflections that belong to water by using the attributes of $amp_{DensRatio}$ and $\sigma(z)$. The attributes are calculated within the 3D ALS point cloud. The main novelty of this method is the use of modeled laser shot dropouts, which mainly occur on water and vegetation. The relation between low amplitudes and dropouts combined with the standard deviation of height values within a search radius of a point provides significant information to distinguish water and land. For the multi-temporal analysis of different ALS campaigns of the same area the amplitude correction and radiometric adjustment are required. The same classification thresholds can be applied to data sets with corrected and radiometric adjusted amplitudes, improving the transferability and comparability to other data sets. A terrestrial orthophoto mosaic is used to check the thresholds for the calculated attributes by visual inspection. A classification accuracy of 95 % correctly derived water reflections was reached.

Literaturverzeichnis

[1] *A.S. Antonarakis, K.S. Richards, and J. Brasington:* Object-based land cover classification using airborne LiDAR. Remote Sensing of Environment, 112(6):2988-2998, 2008.

[2] *C. Briese, B Höfle, H. Lehner, W. Wagner, M. Prenningbauer, and A. Ullrich:* Calibration of Full-Waveform Airborne Laser Scanning Data for Object Classification. In: Proceedings of SPIE – The International Society for Optical Engineering, volume 6950, page 8. SPIE, 2008. DOI: 10.1117/12.781086.

[3] *R. Brügelmann and A.E. Bollweg:* Laser altimetry for river management. In International Archives of Photogrammetry, Remote Sensing and Spatial Information Sciences, Vol. XXXV, B2, pages 234-239, Istanbul, 12-23 July 2004.

[4] *A. Brzank and C. Heipke:* Classification of Lidar Data into water and land points in coastal areas. In: International Archives of Photogrammetry, Remote Sensing and Spatial Information Sciences, Vol. XXXVI, 3, pages 197-202, Bonn, 20-22 September 2006.

[5] *A. Brzank, C. Heipke, J. Goepfert, and U. Soergel:* Aspects of generating precise digital terrain models in the Wadden Sea from lidar – water classification and structure line extraction. ISPRS Journal of Photogrammetry and Remote Sensing, 63(5):510-528, 2008.

[6] *S. Clode, F. Rottensteiner, and P. Kootsookos:* Improving City Model Determination by Using Road Detection from LIDAR Data. In: International Archives of the Photogrammetry, Remote Sensing and Spatial Information Sciences Vol. XXXVI – 3/W24, pages 159-164, Vienna, Austria, 2005.

[7] *J.F. Crétaux and C. Birkett:* Lake studies from satellite radar altimetry. Comptes Rendus Geosciences, 338(14-15):1098-1112, 2006.

[8] *T. Geist and J. Stötter:* Documentation of glacier surface elevation change with multi-temporal airborne laser scanner data – case study: Hintereisferner and Kesselwandferner, Tyrol, Austria. Zeitschrift für Gletscherkunde und Glazialgeologie, 41:77-106, 2007.

[9] *G. C. Guenther, M. W. Brooks, and P. E. LaRocque:* New Capabilities of the SHOALS Airborne Lidar Bathymeter. Remote Sensing of Environment, 73(2):247-255, 2000.

[10] *D. K. Hall:* Remote sensing applications to hydrology: imaging radar. Hydrological Sciences Journal, 41(4):609-624, 1996.

[11] *B. Höfle:* Detecting and Utilizing the Information Potential of Airborne Laser Scanning Point Cloud and Intensity Data by Developing a Managment and Analysis System. PhD thesis, Institut für Geographie, Universität Innsbruck, 2007.

[12] *B. Höfle, T. Geist, M. Rutzinger, and N. Pfeifer:* Glacier surface segmentation using airborne laser scanning point cloud and intensity data. In: International Archives of Photogrammetry, Remote Sensing and Spatial Information Sciences, Vol. XXXVI, 3/W52, page on CD, Espoo, Finland, 12-14 September 2007.

[13] *B. Höfle and N. Pfeifer:* Correction of laser scanning intensity data, data and model-driven approaches. ISPRS Journal of Photogrammetry & Remote Sensing, 62(6):415-433, 2007.

[14] *B. Höfle, N. Pfeifer, C. Ressl, M. Rutzinger, and M. Vetter:* Water surface mapping using airborne laser scanning elevation and signal amplitude data. In: Geophysical Research Abstracts, volume 10, 2008.

[15] *B. Höfle, M. Vetter, N. Pfeifer, G. Mandlburger, and J. Stötter:* Water surface mapping from airborne laser scanning using signal amplitude and elevation data. Earth Surface Processes and Landforms (Special Issue "Remote Sensing of Rivers"), page 15, 2009. in Press.

[16] *J. L. Irish and W. J. Lillycrop:* Scanning laser mapping of the coastal zone: the SHOALS system. ISPRS Journal of Photogrammetry & Remote Sensing, 54(2-3):123-129, 1999.

[17] *A. V. Jelalian. Laser Radar Systems. Artech House Publishers, 1992.*

[18] *J. R. Jensen:* Remote sensing of the environment: an earth resource perspective. Prentice Hall Series in Geographic Information Sciences, 2 edition, 2007.

[19] *S. Kaasalainen, A. Kukko, T. Lindroos, P. Litkey, H. Kaartinen, J Hyyppä, and E. Ahokas:* Brightness measurements and calibration with airborne and terrestrial laser scanners. IEEE Transactions on Geoscience and Remot Sensing, 46(2):528-534, 2008.

[20] *H. Kager, F. Rottensteiner, M. Kerschner, and P. Stadler:* Orpheus 3.2.1 user manual. Technical report, Institute of Photogrammetry and Remote Sensing, Vienna University of Technology., 2002.

[21] *R. Katzenbeisser and S. Kurz:* Airborne Laser-Scanning, ein Vergleich mit terrestrischer Vermessung und Photogrammetrie. Photogram- metrie, Fernerkundung, Geoinformation, 3:179-188, 2004.

[22] *K. Kraus and N. Pfeifer:* Determination of terrain models in wooded areas with airborne laser scanner data. ISPRS Journal of Photogrammetry & Remote Sensing, 53(4):193-203, 1998.

[23] *G. Mandlburger and H. Brockmann:* Modelling a watercourse DTM based on airborne laserscanner data – using the example of the River Oder along the German/Polish Border. In: OEEPE Workshop on Airborne Laserscanning and Interferometric SAR for Detailed Digital Terrain Models, Stockholm, 2001.

[24] *G. Mandlburger, C. Hauer, B. Höfle, H. Habersack, and N. Pfeifer:* Optimisation of LiDAR derived terrain models for river flow modelling. Hydrology and Earth System Sciences Discussion, 5(6):3605 – 3638, 2008.

[25] *W. Marcus and M. Fonstad:* Optical remote mapping of rivers at sub-meter resolutions and waters extents. Earth Surface Processes and Landforms, 33(1):4-24, 2008.

[26] *L. A. K. Mertes:* Remote sensing of riverine landscapes. Freshwater Biology, 47:799-816, 2002.

[27] *Optech:* Optech Incorporated. www.optech.ca, 28.08.2008.

[28] *M. Rutzinger:* Object Detection in Airborne Laser Scanning Data in Urban Environments. PhD thesis, Insitut für Geographie, Universität Innsbruck, 2008.

[29] *T. J. Schmugge, W. P. Kustas, J. C. Ritchie, T. J. Jackson, and A. Rango:* Remote sensing in hydrology. Advances in Water Resources, 25(8-12):1367-1385, 2002.

[30] *G. Schumann, R. Hostache, C. Puech, L. Hoffmann, P. Matgen, F. Pappenberger, and L. Pfister:* High-Resolution 3-D Flood Information From Radar Imagery for Flood Hazard Management. IEEE Transactions on Geoscience and Remote Sensing, 45(6):1715-1725, 2007.

[31] *G. Sithole and G. Vosselman:* Experimental comparison of filter algorithms for bare-Earth extraction from airborne laser scanning point clouds. ISPRS Journal of Photogrammetry & Remote Sensing, 59(1-2):85-101, 2004.

[32] *S. L. Ustin:* Remote Sensing for Natural Resources Management and Environmental Monitoring, volume 4 of Manual of Remote Sensing, chapter Rivers and Lakes, pages 345-400. American Society for Photogrammetry and Remote Sensing, 3 edition, 2004.

[33] *M. Vetter, B. Höfle, G. Mandlburger, and M. Rutzinger:* Integration von Flussquerpro- filen in Airborne Laserscanning Geländemodelle für hydraulische Fragestellungen mit GRASS GIS. In: Angewandte Geoinformatik 2008, Beiträge zum 20. AGIT-Symposium, pages 382-391, Salzburg, Juli 2008.

[34] *G. Vosselman:* 3-D Reconstruction of Roads and Trees for City Modelling. In: International Archives of Photogrammetry, Remote Sensing and Spatial Information Sciences, Vol. XXXIV, 3/W13, pages 231-236, Dresden, Germany, 8-10 October 2003.

[35] *W. Wagner, A. Ullrich, T. Melzer, C. Briese, and K. Kraus:* From Single-Pulse to Full-Waveform airborne laser scanners potential and practical challenges. In: International Archives of Photogrammetry, Remote Sensing and Spatial Information Sciences, Vol.XXXV, B3, pages 201-206, Istanbul, Turkey, 12-23 July 2004.

[36] *W. L. Wolfe and G. J. Zissis:* The infrared handbook. The Infrared Informatinon Analysis Center. Environmental Research Insitute of Michigan, 1989.

Address of authors

Mag. Michael Vetter, Department of Geography, University of Innsbruck, Innrain 52, 6020 Innsbruck, Austria
e-mail: michael.vetter@uibk.ac.at
and
Institute of Photogrammetry and Remote Sensing, Vienna University of Technology, Gußhausstraße 27 – 29, 1040 Vienna, Austria
E-mail: mv@ipf.tuwien.ac.at

Mag. Dr. Bernhard Höfle, Christian Doppler Laboratory „Spatial Data from Laser Scanning and Remote Sensing", Institute of Photogrammetry and Remote Sensing, Vienna University of Technology, Gußhausstraße 27 - 29, 1040 Vienna, Austria
E-mail: bh@ipf.tuwien.ac.at

Mag. Dr. Martin Rutzinger, International Institute for Geo-Information Science and Earth Observation, Hengelosestraat 99, 7514 AE Enschede, The Netherlands
E-mail: rutzinger@itc.nl